Roles of upper-level processes in tropical cyclogenesis

Da-Lin Zhang[1] and Lin Zhu[1]

[1] Previous studies have focused mostly on the impact of lower-level vorticity growth and other lower-level processes on tropical cyclogenesis (TCG). In this study, the importance of upper-level processes in TCG is studied in terms of the minimum sea-level pressure (MSLP) changes with two cases exhibiting different warm-core heights and vorticity structures due to their developments in the respective weak- and strong-sheared environment. Results show that the upper-level warming could account for more than 75% the MSLP changes in both cases. Widespread deep convection during the early TCG stage tends to warm the upper troposphere and induce meso-α-scale surface pressure falls. Upper-level flow and vertical wind shear (VWS) will suppress the formation of a warm core due to the presence of weak inertial stability, whereas the development of upper-level divergent outflows favors its formation. Results also show that TCG is triggered when the upper-level warming amplitude and depth increase as a result of weak or significantly reduced ventilation and VWS aloft. Results suggest that both the upper- and low-level processes be considered in the understanding and prediction of TCG. **Citation:** Zhang, D.-L., and L. Zhu (2012), Roles of upper-level processes in tropical cyclogenesis, *Geophys. Res. Lett.*, *39*, L17804, doi:10.1029/2012GL053140.

1. Introduction

[2] Tropical cyclogenesis (TCG) from a weak atmospheric disturbance requires synergistic interactions among different physical processes that can generate a self-sustained, warm-core vortex of at least tropical storm intensity. We define TCG as the two stages during which a low-level disturbance exhibits little intensity changes (e.g., less than a 5 hPa day^{-1} drop in the minimum sea-level pressure (MSLP)), i.e., a pre-genesis stage, followed by a stage of significant intensification (SI, e.g., greater than a 0.5 hPa hr^{-1} drop). The physical processes leading to SI or the onset of TCG are often of major concern. Some climatologically necessary conditions for TCG include an underlying warm sea-surface temperature (SST) of at least 26°C, a finite-amplitude low-level cyclonic disturbance, weak vertical wind shear (VWS), and low- to midlevel moist columns [*Gray*, 1979]. The essence of warm SST was later described in the context of the wind-induced surface heat exchange process [*Emanuel*, 1986; *Rotunno and Emanuel*, 1987], in which self-induced latent and sensible heat transfer from the warm ocean to the atmosphere acts to spin up the finite amplitude disturbance.

[3] Given the above favorable background conditions, large-scale circulations appear to determine where TCG may occur, as demonstrated by the recent success of global models in predicting tropical cyclone (TC) tracks. They include easterly waves [*Molinari et al.*, 1999], monsoon troughs [*Harr and Elsberry*, 1996], upper-level potential vorticity anomalies [*Davis and Bosart*, 2001], mixed Rossby-gravity waves [*Aiyyer and Molinari*, 2003], the Saharan air layer [*Dunion and Velden*, 2004], breakdown of the inter-tropical convergence zone [*Nieto Ferreira and Schubert*, 1997; *Wang and Magnusdottir*, 2006; *Kieu and Zhang*, 2008], and mesoscale convective systems (MCSs) [*Zhang and Bao*, 1996a, 1996b; *Zhang et al.*, 2011].

[4] More attention during the past two decades has been paid to mesoscale processes leading to TCG as a result of the rapid growth in computing power and achievements in mesoscale field observations. Most studies have examined the bottom-up and top-down vorticity growth hypotheses. Although the top-down hypothesis contains some plausible scenarios associated with TCG [*Ritchie and Holland*, 1997; *Bister and Emanuel*, 1997], prevailing studies tend to confirm the bottom-up growth of cyclonic vorticity. *Zhang and Bao* [1996b] find that a midlevel mesoscale convective vortex (MCV) could provide necessary quasi-balanced forcing for the initiation and organization of deep convection, which in turn causes the amplification of the low-level cyclonic vorticity in the presence of intensifying boundary-layer convergence. This bottom-up vorticity growth mechanism was later advanced by *Hendricks et al.* [2004] and *Montgomery et al.* [2006] by including convective "vortical hot towers (VHTs)" as the building blocks of TCs, and TCG occurs as a result of the mean–eddy interaction, i.e., an axisymmetrization process [*Montgomery and Enagonio*, 1998]. Recently, *Dunkerton et al.* [2009], *Montgomery et al.* [2010], and *Wang et al.* [2010] develop an innovative framework in which TCG occurs as a result of both the low-level vorticity growth and moistening within a quasi-closed Lagrangian circulation associated with an easterly wave, the so-called wave's pouch hypothesis.

[5] The trigger of SI has also received some attention in recent TC studies. Using a cloud-resolving simulation of a TC-like vortex with idealized initial conditions, in which no mean wind is present, *Nolan* [2007] shows that convectively generated near-saturated conditions in the core region and increased vortex rotation are responsible for the trigger of SI. *Kieu and Zhang* [2008] find that the trigger of SI of Tropical Storm Eugene (2005) results from the merging of two midlevel MCVs. *Ritchie and Holland* [1997] also note the merging of multiple MCVs during the genesis of Typhoon Irving (1992). *Hogsett and Zhang* [2011] show that the SI of Typhoon Chanchu (2006) occurs as its associated vertically tilted vortex becomes upright.

[6] It is evident that the previous studies have focused mostly on the low- to midlevel processes leading to TCG. In this study, we will test the hypothesis that upper-level

---

[1]Department of Atmospheric and Oceanic Science, University of Maryland, College Park, Maryland, USA.

Corresponding author: D.-L. Zhang, Department of Atmospheric and Oceanic Science, University of Maryland, College Park, MD 20742-2425, USA. (dalin@atmos.umd.edu)
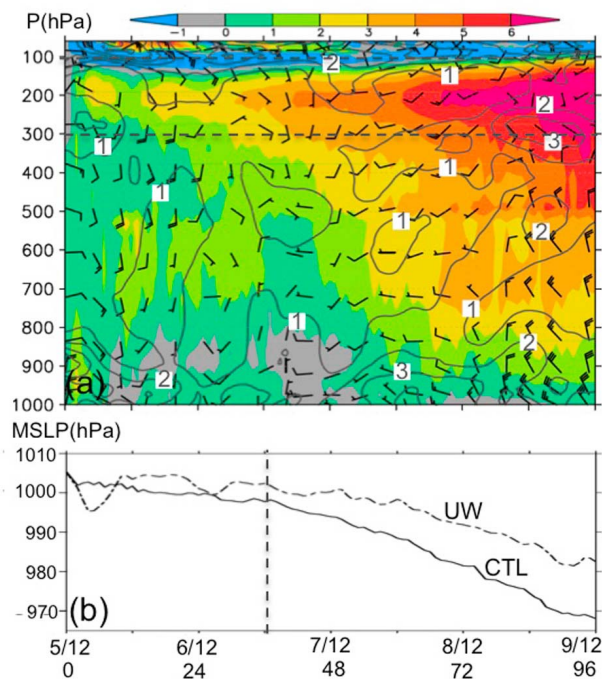
Figure 1. (a) Time-height cross section of temperature changes ($\delta T(z, t)$, °C, shaded) and the (500 km × 500 km) areal-averaged local VWS (every 10^{-3} s^{-1}, contoured) superposed with the storm-relative flows (a full barb is 5 m s^{-1}), all at the surface circulation center from the 96-h simulation of Typhoon Nari (2001) at 36-km and 1 hourly resolutions, where $\delta T(z, t)$ is defined with respect to the vertical temperature profile ($T(z)$) at the model initial time. (b) Time series of the control-simulated MSLP (solid, CTL), and the hydrostatically estimated MSLP (dashed, UW) by including $\delta T(z, t) > 0$ in the 100–300 hPa layer (dashed lines). The UTC date/hour and model hour are provided beneath Figure 1b. The vertical-dashed lines in Figure 1b denote the onset of SI.

processes (e.g., convectively generated compensating subsidence warming, subsidence warming in the wake region of MCSs, VWS and ventilation) play critical roles in TCG. This will be done using the nested-grid, cloud-resolving simulations of two TCG cases, i.e., the genesis of Typhoon Nari (2001) from an MCS/MCV in a quasi-barotropic environment [*Zhang et al.*, 2011, hereinafter referred to as ZTY11] and the genesis of Typhoon Chanchau (2006) from a westerly wind burst (WWB) with strong VWS [*Hogsett and Zhang*, 2010, 2011, hereinafter referred to as HZ10 and HZ11, respectively]. This study is motivated by the recent work of *Zhang and Chen* [2012, hereinafter referred to as ZC12] that the formation of an upper-level warm core in a weak environmental flow could hydrostatically account for the rapid MSLP falls of a TC. The next two sections show how the upper-level processes determine the genesis of Typhoons Nari (2001) and Chanchau (2006), respectively, in terms of the MSLP falls. The trigger of SI will also be examined.

2. Genesis of Typhoon Nari (2001): An "Ideal" Storm

[7] ZTY11 shows that Nari could be traced 5 days back to a diurnally convection-varying MCS (on September 1) with

increasing cyclonic vorticity and relative humidity in the lower troposphere, as it moved over a warm ocean (with the SSTs of greater than 29°C) under the influence of a subtropical high. Genesis of Nari did not begin until 1200 UTC 5 September when a closed surface circulation developed as the 200–850 hPa VWS was reduced to less than 5 m s^{-1}. Thus, this is an "ideal" storm to examine only the roles of upper-level warming in TCG. However, the passage of a weak surface cold front interrupted the possible genesis by altering convective organization during the period of 2100 UTC 5–1200 UTC 6 September. A successful 96-h (i.e., 1200 UTC 5 to 1200 UTC 9 September) simulation of Nari's track and intensity was obtained using the Penn State/NCAR MM5 model with the finest grid size of 1.33 km (ZTY11). Of relevance to this study is that the simulated storm exhibits a 4-hPa drop in MSLP during the first 36-h simulation and a 0.5 hPa hr^{-1} SI rate for the remaining 60-h period (Figure 1b).

[8] Figure 1a shows the time-pressure (*t-p*) cross section of perturbation temperatures ($\delta T(z, t)$) with respect to the vertical temperature profile ($T(z, 0)$) at the model initial time, superimposed with the storm-relative flows (SRFs) and the areal-averaged local VWS, all taken at the surface circulation center. One can see that deep convection in the core region begins to produce a deep-layer (i.e., 900–120 hPa) of warming after 3 h into the simulation, with its peak magnitude located at 200 hPa, which is 50–80 hPa below the tropopause. Note that the word "warming" is used herein to imply a positive temperature change(s) with respect to $T(z, 0)$ in the storm-relative framework. In addition, we use the model hours instead of UTC, except in figures or figure captions, to discuss the structures and evolution of the simulated features. Some cooling also appears in the lower stratosphere as a result of convective lifting of the tropopause. The above results are intuitively understandable because deep convection tends to stabilize atmospheric columns by warming the upper troposphere through compensation subsidence and cooling the lower troposphere [*Fritsch and Chappell*, 1980]. Such subsidence warming is often peaked slightly below the tropopause where convective updrafts lose buoyancy and detrain [*Hoxit et al.*, 1976].

[9] In general, the warming column increases in magnitude and expands in depth with time, more downward towards the top of the boundary layer (at about 900 hPa). Of interest is that the warming core remains at 200 hPa throughout the 96-h period. In particular, the upper-level warming rate increases more significantly near 36 h (i.e., a 1°C increase during the first 30-h compared to the same amount increase during the 30–36 h), which coincides with the onset of SI or TCG of Nari (Figure 1b). Furthermore, the lower half of the troposphere experiences little warming prior to the onset of TCG. Based on the work of ZC12, we may attribute the onset of TCG to the increased upper-level warming rate in the core region.

[10] To see the above point, Figure 1b is plotted following the same procedures as those described by ZC12. That is, (a) the time series of the control-simulated MSLP (CTL) is reproduced by integrating the hydrostatic equation from the model top downward using the total temperature (i.e., $T(z, t) = T(z, 0) + \delta T(z, t)$); and (b) repeat step (a) to obtain the time series of MSLP but with the upper-level warming only, i.e., by including the sublayers with $\delta T(z, t) > 0$ in the 100–300 hPa layer (curve UW). Note that the cooling sublayers in the 100–300 hPa layer are excluded in curve UW to isolate
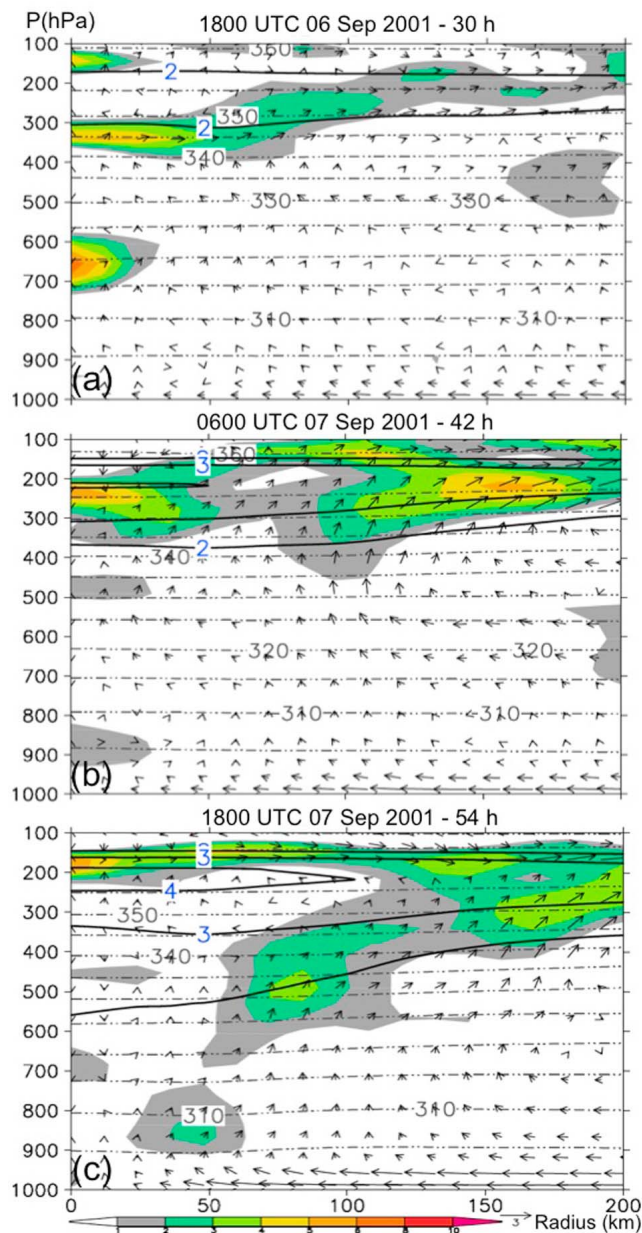
Figure 2. Radius – pressure cross section of divergence (shaded, 10^{-5} s^{-1}), temperature changes ($\delta T(z, t)$, solid, every 1°C) with respect to the initial values, and potential temperature (dashed, every 5 K), taken from (a) 30-h, (b) 42-h, and (c) 54-h simulations of Typhoon Nari (2001), corresponding to 6 h prior to, 6 h after and 18 h after the onset of SI, respectively. Superimposed are in-plane flow vectors (m s^{-1}, radial flows scaled by an arrow beneath the frame (Figure 2c); vertical motions are multiplied by 10).

the impact of the warming core on the MSLP falls. On average, the upper-level warming accounts for about 78% of the MSLP changes, including *the mean slow deepening rate during the first 36 h and the subsequent* 0.5 hPa hr^{-1} *SI rate.* However, the MSLP is elevated, especially for the first 9 h, due to the exclusion of the above-mentioned cooling sublayers. It follows that the increased upper-level warming rate near 36 h explains well the trigger of Nari's SI. This confirms further that warming at lower temperatures aloft is more effective than the lower-level warming in hydrostatically inducing MSLP falls (ZC12).

[11] It is apparent from Figure 1a that the deep warming layer is characterized by weak VWS (i.e., $\sim 10^{-3}$ s^{-1}) and weak SRFs (i.e., less than 5 m s^{-1}), especially in the upper warming layer. More pronounced VWS takes place in the lowest 150 hPa and above 120 hPa, and the SRFs of larger than 10 m s^{-1} occur in the midtroposphere prior to the onset of TCG or after reaching typhoon intensity. Obviously, the presence of weak SRFs and VWS in the core region would prevent the upper-level warm air from ventilation and the warm column from tilting downshear, thereby facilitating hydrostatically the maintenance and falls of the central MSLP.

[12] In order to understand the formation of the upper-level warming, Figure 2 shows the (axisymmetric) radius - pressure (R-p) structures of the warming, divergence and secondary circulations of the simulated Nari at three different stages: about 6 h prior to and 6 h after the onset of SI plus its mature stage. We see a typical in- up- and outward circulation, which becomes better organized as the storm enters the mature stage. The upper outflow layer experiences significant warming, even more than 400 km away from the center (see Figure S1 in the auxiliary material), indicating the important ventilation effects of SRFs.[1] Because of little cooling occurring in the lower troposphere, the upper-level widespread warming could hydrostatically induce meso-α-scale MSLP falls (Figure S1). This result suggests that *one of the roles of widespread deep convection during the pre-genesis stage is to warm the upper troposphere and induce meso-α-scale MSLP falls* (Figure S1), albeit at very slow rates. Such mesoscale MSLP falls would enhance the low-level moisture convergence, further convective development and the low-level vorticity growth, given larger-scale favorable conditions.

[13] Note that the upper-level warming core takes place in the same layer as the divergent outflow extending well into the far outer region. We hypothesize that this upper divergent outflow tends to help protect the inner warming core from ventilation by environmental flows during TCG (Figure S1). Whether or not the warm core could be maintained would depend on the intensity of (asymmetric) SRFs and the corresponding balanced flows. More importantly, a large portion of the subsidence warming aloft during the pre-genesis stage would be dispersed away by inertial gravity waves due to the presence of large static stability. We may speculate that only after isentropic surfaces aloft in the core region begin to descend more downward with a balanced circulation, can the warming accelerate to trigger the SI of Nari (cf. Figures 2a and 2b). Indeed, we see a meso-β-scale warming core of about 4°C within the radius of 50 km at 6 h after the onset of SI (Figure 2b). This warming core grows in intensity and volume with time during SI, under the protection of a deep-layer divergent circulation in the outer region (Figures 2b and 2c).

3. Genesis of Typhoon Chanchau (2006) Under Intense Vertical Wind Shear

[14] HZ11 shows that the pre-Chanchu vortex intensified over a warm ocean (with the SSTs of more than 29°C) on the cyclonic side of a WWB near the equator. An 11-day (i.e.,

---
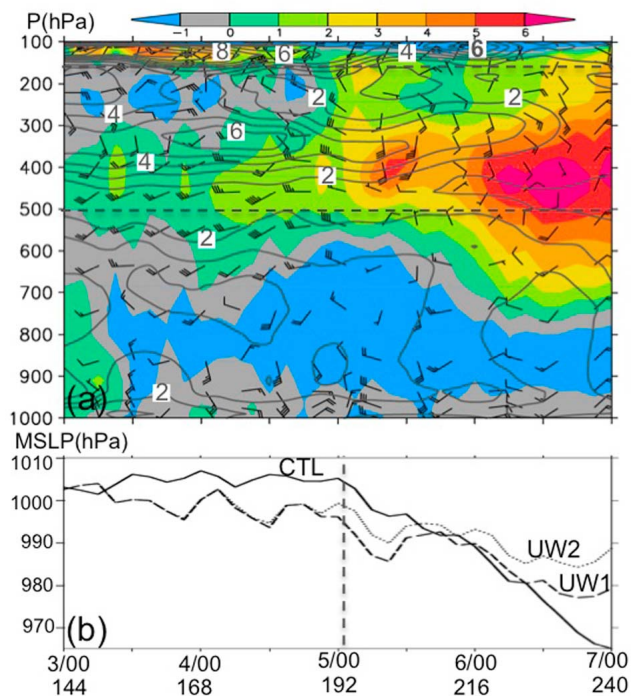
Figure 3. As in Figure 1 but for a 96-h time window from the 11-day simulation of Typhoon Chanchu (2006) at the 18-km and 3 hourly resolutions. (a) Dashed lines indicate the warming (166–500 hPa) layer with $\delta T(z, t) > 0$ that is used to calculate (b) the MSLP time series, i.e., curve UW1. Curve UW2 in Figure 3b denotes the calculated MSLP time series with $\delta T(z, t) > 0$ in the 300–500 hPa layer.

0000 UTC 27 April to 0000 UTC 8 May 2006) simulation of the storm, using the Weather Research and Forecast model with the finest grid length of 2 km, reveals that the pre-Chanchu vortex tilts westward over a horizontal distance of more than 500 km in the 400–900 hPa layer, and it is characterized by a weak warm column above and an elevated cold-cored layer below with large VWS across the vortex layer prior to SI, and a surface-based warm-core circulation in the lowest 300-hPa layer (see HZ11, Figure 10). Although a well-defined surface vortex begins to appear at 72 h, an SI rate of about 0.8 hPa hr^{-1} does not occur until 5 days later, i.e., at 192 h. The onset of SI is triggered, when the vertically tilted midlevel vortex is aligned with the surface-based one. The storm-scale rotation is peaked near 600 hPa (see HZ11, Figure 9), as compared to 900 hPa in Nari (see ZTY11, Figure 16). Thus, Chanchau's pronounced baroclinicity with the larger-scale VWS of more than 15 m s^{-1} in the 400–900 hPa layer provides a different test from Nari's case for the relationship between the upper-level warming and flows, and TCG.

[15] Figure 3 shows a 96-h time window of the same fields as those in Figure 1 except for Chanchau, covering a pre-genesis and an SI stage of 48 h each, respectively. Unlike Nari, the upper-level warming is peaked in the 400–450 hPa layer (Figure 3a), and it is hydrostatically related to the tilted vortex centered near 500 hPa as a result of mesoscale subsidence in the wake region of an MCS (see HZ11, Figures 3–5

and 10). The peak warming increases slowly during the pre-genesis stage (i.e., only 2–3°C between 144 and 192 h), but markedly after the onset of SI (e.g., 3–4°C during the 12-h period of 192–204 h), which corresponds to the slow and more rapid amplification of the surface-based vortex, respectively. (Note that the midlevel vortex does not exert more significant influence on the warming core until it is vertically aligned with the surface based vortex.) Moreover, the 150–300 hPa layer even exhibits weak cooling, due to the sublimative cooling of cloud hydrometeors in the stratiform region (HZ11), until 192 h when a sign change to warming occurs. Below 600 hPa the surface-based vortex experiences 1–2°C cooling with respect to the 144-h warm column. Overall, the weak upper-level warming offsets the cooling in the layers underneath and aloft, accounting for the nearly flat MSLP time series for at least 48 h prior to SI (Figure 3b).

[16] This different altitude in the peak warming from Nari's is more or less determined by the vertical distribution and evolution of VWS and SRFs in the core region. That is, the upper half of the troposphere is characterized by intense VWS with the peak magnitude of greater than 6×10^{-3} s^{-1} centered at 320 hPa and intense SRFs with the peak magnitude of greater 20–25 m s^{-1} in the peak warming layer until the onset of SI (Figure 3a). However, the upper-level VWS and SRFs begin to weaken after 192 h, which coincides with the above-mentioned increases in the warming rate and the vertical alignment of the two vortices (HZ11). Of interest is that the warming depth near this time extends upward to 150 hPa, where the tropopause is roughly located. This indicates that compensating subsidence warming by deep convective updrafts begins to contribute to TCG from this time on. Note the development of a weak SRF (150–300 hPa) layer above an intense SRF (300–450 hPa) layer during the 192–210 h period. This wind structure is associated with the top portion of the Chanchau vortex that still remains vertically tilted, as indicated by directional changes from less rotating westerly-to-northwesterly to more rotating southerly-to-southeasterly SRFs during the early SI period. Because of this vertical tilt, only part of the top warming columns is overlaid with the central portion of the surface circulation. This vertical tilt diminishes after 228 h at which time more pronounced warming in the core region occurs immediately beneath the tropopause.

[17] Figure 3b shows the impact of the upper-level warming on the genesis of Chanch, which is plotted following the same procedures as those described in section 2. To compare more meaningfully with Nari's case, an equal $\delta(\ln p) = 3$ (i.e., 166–500 hPa) layer is used to represent the upper-level influences (curve UW1). Indeed, including the upper-level warming in this equal δ lnp layer produces similar influences on the MSLP time series between the two typhoons. Namely, the 166–500 hPa layer warming accounts for about 8 hPa drops in MSLP from that in the CTL during the first 48 h, and almost all of the 0.8 hPa hr^{-1} SI rate during the periods of 192–204 h and 210–228 h. Moreover, it is the increased warming depth and rate near 192 h that trigger the SI of Chanchau (cf. Figures 3a and 3b). Note, though, that pronounced fluctuations in the MSLP time series, which also appear to a certain extent in Figure 1b, are directly caused by the corresponding fluctuations in the
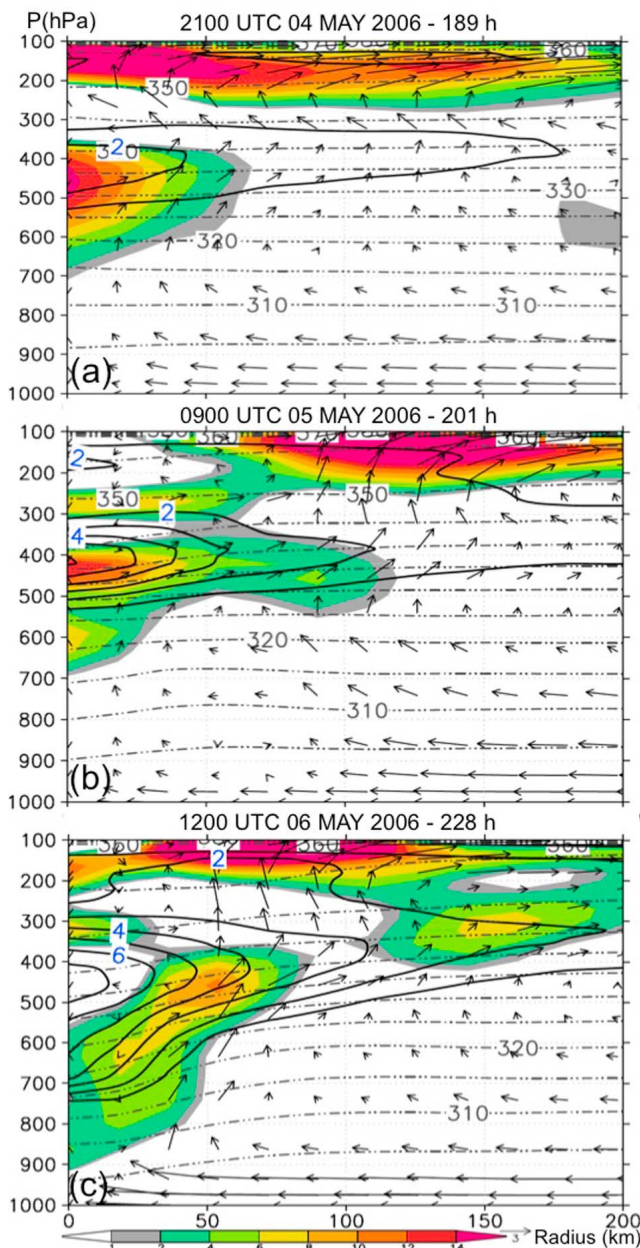
Figure 4. As in Figure 2, but temperature changes (δT(z, t), solid, every 1°C) are calculated with respect to the 144-h temperature field from (a) 189-h, (b) 201-h, and (c) 228-h simulations of Typhoon Chanchu (2006). Vertical motions are multiplied by 5.

upper-level warming amplitude as a result of horizontally elliptic and vertically less coherent vortex structures under the influence of intense VWS (HZ11). If only the peak warming layer of 300–500 hPa is considered (curve UW2), the storm is 4–5 hPa and 8–9 hPa weaker than that shown in UW1 near the onset of SI and the end of the 240-h integration, respectively; and on average SI does not occur. This result shows further the more effectiveness of the higher-level warming than the lower-level warming in inducing MSLP falls.

[18] The axisymmetric vertical structures of the warming and secondary circulations are given in Figure 4, showing the

intensification of a warm core near 400 hPa within the radius of more than 200 km from 2°C at 189 h to 6°C at 201 h, and 7°C at 228 h. Of significance is the presence of two distinct divergent outflow layers: one in the same layer as the warming core and the other slightly beneath the tropopause (Figures 4a and 4b). The latter is clearly related to the cloud-top detrainment of deep convection, like that shown in Figure 2, whereas the former is associated with supergradient flows resulting from the upward transport of absolute angular momentum at the maximum rotational level of the MCV [*Zhang et al.*, 2001]. Thus, most of the warming core at 450 hPa does not seem to be generated directly by compensating subsidence from deep updrafts, but by mesoscale subsidence in the wake region (HZ11). Despite the contribution of convectively generated subsidence, much slower warming occurs in the higher (divergent) layer than that in the warming-core layer after the onset of SI. This could be attributed partly to the rapidly reduced inertial stability higher up and partly to the more rapid energy dispersion of internal gravity waves aloft.

4. Concluding Remarks

[19] In this study, the roles of upper-level processes in TCG are examined in terms of MSLP changes with two previously studied cases that developed under the respective weak- and strong-VWS environment. Results show that the upper-level warming accounts for more than 75% of the MSLP changes in both cases (with the correlation coefficients of 0.97 and 0.92 for Nari and Chanchau, respectively), and indicate that the higher-level warming is more effective than the lower-level one in hydrostatically inducing MSLP falls. Widespread deep convection during the pre-genesis stage tends to warm the upper troposphere and induce meso-α-scale surface pressure falls, thereby facilitating the low-level convergence and vorticity growth. Results also show that intense upper-level VWS and SRFs tend to suppress the formation of an upper-level warm core due to the presence of little inertial stability, whereas the development of upper-level divergent outflows favors its formation. We find that the onset of TCG is triggered when more rapid warming and increased warming depth take place in the upper troposphere where both VWS and SRFs are weak or significantly reduced. This often occurs when the upper-level warm core and lower-level vortex become more vertically coherent. Thus, we may conclude that given warm SSTs and other favorable conditions, the upper-level processes, especially, VWS and SRFs, play critical roles in determining the onset of TCG.

[20] Of course, the above conclusion does not imply that the lower-level processes, as examined by previous studies, are not important in TCG, but indicates that both the upper- and lower-level processes need to be taken into account in the understanding and prediction of TCG. In our view, the upper-level warming helps precondition the lower-level TC-scale flows, by inducing meso-α-scale surface pressure falls, such that a meso-α-scale low-level convergence could be enhanced to facilitate the growth of cyclonic vorticity (from VHTs to meso-β-scale vortices) from the bottom upward via stretching. Based on the above results, we may hypothesize that *even with all favorable low-level conditions, TCG may not likely occur if an upper-level warm column could not be established due to the detrimental impact of intense upper-*

level VWS and ventilation. Nevertheless, more detailed case studies are needed to test the above hypothesis, and examine the different roles of the upper- and lower-level processes and their interaction in TCG.

[22] The Editor thanks the anonymous reviewer for assistance in evaluating this paper.

References

Aiyyer, A., and J. Molinari (2003), Evolution of mixed Rossby-gravity waves in idealized MJO environments, *J. Atmos. Sci.*, *60*, 2837–2855, doi:10.1175/1520-0469(2003)060<2837:EOMRWI>2.0.CO;2.

Bister, M., and K. A. Emanuel (1997), The genesis of Hurricane Guillermo: TEXMEX analyses and a modeling study, *Mon. Weather Rev.*, *125*, 2662–2682, doi:10.1175/1520-0493(1997)125<2662:TGOHGT>2.0.CO;2.

Davis, C. A., and L. F. Bosart (2001), Numerical simulations of the genesis of Hurricane Diana (1984). Part I: Control simulation, *Mon. Weather Rev.*, *129*, 1859–1881, doi:10.1175/1520-0493(2001)129<1859:NSOTGO>2.0.CO;2.

Dunion, J. P., and C. S. Velden (2004), The impact of the Saharan air layer on Atlantic tropical cyclone activity, *Bull. Am. Meteorol. Soc.*, *85*, 353–365, doi:10.1175/BAMS-85-3-353.

Dunkerton, T. J., M. T. Montgomery, and Z. Wang (2009), Tropical cyclogenesis in a tropical wave critical layer: Easterly waves, *Atmos. Chem. Phys.*, *9*, 5587–5646, doi:10.5194/acp-9-5587-2009.

Emanuel, K. A. (1986), An air-sea interaction theory for tropical cyclones. Part I: Steady-state maintenance, *J. Atmos. Sci.*, *43*, 585–605, doi:10.1175/1520-0469(1986)043<0585:AASITF>2.0.CO;2.

Fritsch, J. M., and C. F. Chappell (1980), Numerical prediction of convectively driven mesoscale pressure systems. Part II: Mesoscale model, *J. Atmos. Sci.*, *37*, 1735–1762.

Gray, W. M. (1979), Hurricanes: Their formation, structure, and likely role in the tropical cyclones, in *Meteorology Over the Tropical Oceans*, edited by D. B. Shaw, pp. 155–218, R. Meteorol. Soc., London.

Harr, P. A., and R. L. Elsberry (1996), Structure of a mesoscale convective system embedded in Typhoon Robyn during TCM-93, *Mon. Weather Rev.*, *124*, 634–652, doi:10.1175/1520-0493(1996)124<0634:SOAMCS>2.0.CO;2.

Hendricks, E. A., M. T. Montgomery, and C. A. Davis (2004), The role of "vortical" hot towers in the formation of tropical cyclone Diana (1984), *J. Atmos. Sci.*, *61*, 1209–1232, doi:10.1175/1520-0469(2004)061<1209:TROVHT>2.0.CO;2.

Hogsett, W., and D.-L. Zhang (2010), Genesis of Typhoon Chanchu (2006) from a westerly wind burst associated with the MJO. Part I: Evolution of a vertically tilted precursor vortex, *J. Atmos. Sci.*, *67*, 3774–3792, doi:10.1175/2010JAS3446.1.

Hogsett, W., and D.-L. Zhang (2011), Genesis of Typhoon Chanchu (2006) from a westerly wind burst associated with the MJO. Part II: Roles of deep convection in tropical transition, *J. Atmos. Sci.*, *68*, 1377–1396, doi:10.1175/2010JAS3512.1.

Hoxit, L. R., C. F. Chappell, and J. M. Fritsch (1976), Formation of mesolows or pressure troughs in advance of cumulonimbus clouds, *Mon. Weather Rev.*, *104*, 1419–1428, doi:10.1175/1520-0493(1976)104<1419:FOMOPT>2.0.CO;2.

Kieu, C. Q., and D.-L. Zhang (2008), Genesis of Tropical Storm Eugene (2005) associated with the ITCZ breakdowns. Part I: Observational and modeling analyses, *J. Atmos. Sci.*, *65*, 3419–3439, doi:10.1175/2008JAS2605.1.

Molinari, J., P. K. Moore, and V. P. Idone (1999), Convective structure of hurricanes as revealed by lightning locations, *Mon. Weather Rev.*, *127*, 520–534, doi:10.1175/1520-0493(1999)127<0520:CSOHAR>2.0.CO;2.

Montgomery, M. T., and J. Enagonio (1998), Tropical cyclogenesis via convectively forced vortex Rossby waves in a three-dimensional quasi-geostrophic model, *J. Atmos. Sci.*, *55*, 3176–3207, doi:10.1175/1520-0469(1998)055<3176:TCVCFV>2.0.CO;2.

Montgomery, M. T., M. E. Nicholls, T. A. Cram, and A. Saunders (2006), A "vortical" hot tower route to tropical cyclogenesis, *J. Atmos. Sci.*, *63*, 355–386, doi:10.1175/JAS3604.1.

Montgomery, M. T., L. L. Lussier III, R. W. Moore, and Z. W. Wang (2010), The genesis of Typhoon Nuri as observed during the Tropical Cyclone Structure 2008 (TCS-08) field experiment. Part 1: The role of the easterly wave critical layer, *Atmos. Chem. Phys.*, *10*, 9879–9900, doi:10.5194/acp-10-9879-2010.

Nieto Ferreira, N. R., and W. H. Schubert (1997), Barotropic aspects of ITCZ breakdown, *J. Atmos. Sci.*, *54*, 261–285.

Nolan, D. S. (2007), What is the trigger for tropical cyclogensis?, *Aust. Meteorol. Mag.*, *56*, 241–266.

Ritchie, E. A., and G. J. Holland (1997), Scale interactions during the formation of Typhoon Irving, *Mon. Weather Rev.*, *125*, 1377–1396, doi:10.1175/1520-0493(1997)125<1377:SIDTFO>2.0.CO;2.

Rotunno, R., and K. A. Emanuel (1987), An air-sea interaction theory for tropical cyclones. Part II: Evolutionary study using a nonhydrostatic axisymmetric numerical model, *J. Atmos. Sci.*, *44*, 542–561, doi:10.1175/1520-0469(1987)044<0542:AAITFT>2.0.CO;2.

Wang, C.-C., and G. Magnusdottir (2006), The ITCZ in the central and eastern Pacific on synoptic time scales, *Mon. Weather Rev.*, *134*, 1405–1421, doi:10.1175/MWR3130.1.

Wang, Z., M. T. Montgomery, and T. J. Dunkerton (2010), Genesis of pre-hurricane Felix (2007). Part I: The role of the easterly wave critical layer, *J. Atmos. Sci.*, *67*, 1711–1729, doi:10.1175/2009JAS3420.1.

Zhang, D.-L., and N. Bao (1996a), Oceanic cyclogenesis as induced by a mesoscale convective system moving offshore. Part I: A 90-h real-data simulation, *Mon. Weather Rev.*, *124*, 1449–1469, doi:10.1175/1520-0493(1996)124<1449:OCAIBA>2.0.CO;2.

Zhang, D.-L., and N. Bao (1996b), Oceanic cyclogenesis as induced by a mesoscale convective system moving offshore. Part II: Genesis and thermodynamic transformation, *Mon. Weather Rev.*, *124*, 2206–2226, doi:10.1175/1520-0493(1996)124<2206:OCAIBA>2.0.CO;2.

Zhang, D.-L., and H. Chen (2012), Importance of the upper-level warm core in the rapid intensification of a tropical cyclone, *Geophys. Res. Lett.*, *39*, L02806, doi:10.1029/2011GL050578.

Zhang, D.-L., Y. Liu, and M. K. Yau (2001), A multiscale numerical study of Hurricane Andrew (1992). Part IV: Unbalanced flows, *Mon. Weather Rev.*, *129*, 92–107, doi:10.1175/1520-0493(2001)129<0092:AMNSOH>2.0.CO;2.

Zhang, D.-L., L. Tian, and M.-J. Yang (2011), Genesis of Typhoon Nari (2001) from a mesoscale convective system, *J. Geophys. Res.*, *116*, D23104, doi:10.1029/2011JD016640.